Uniform and nonuniform thermal switching of magnetic particles

D. A. Garanin
Physics Department, Lehman College and Graduate School, City University of New York, 250 Bedford Park Boulevard West, Bronx, New York 10468-1589, USA

(Received 11 March 2018; revised manuscript received 2 August 2018; published 16 October 2018)

The pulse-noise approach to systems of classical spins weakly interacting with the bath has been applied to study thermally activated escape of magnetic nanoparticles over the uniform and nonuniform energy barriers at intermediate and low damping. The validity of approximating a single-domain particle by a single spin is investigated. Barriers for a nonuniform escape of elongated particles for the uniaxial model with transverse and longitudinal field have been worked out. Pulse-noise computations have been done for finite magnetic chains. The linear stability of the uniform barrier state has been investigated. The crossover between uniform and nonuniform barrier states has been studied with the help of the variational approach.

DOI: 10.1103/PhysRevB.98.144425

I. INTRODUCTION

Miniaturization of magnetic elements in spintronics and memory applications increases the importance of their thermal stability and puts the question of lifetimes of different magnetic states. These lifetimes are usually related to overcoming energy barriers under the influence of thermal agitation, which becomes increasingly easy for small sizes of magnetic particles, eventually leading to superparamagnetism. On the other hand, elongated magnetic elements, such as stripes and nanopillars, can overcome energy barriers by a nonuniform rotation of the magnetization, for instance, via the motion of a domain wall across them. In this case the energy barrier depends on the cross section but not on the length of the magnetic elements.

The magnetic states in different geometries, taking into account the dipole-dipole interaction (DDI), have been extensively studied within the so-called micromagnetic approach [1] (for a recent reference, see Ref. [2]), considering magnetic materials within the continuous approximation. Initially, this approach was formulated for zero temperature, $T = 0$, but in practice one can use material parameters measured at finite T. Energy barriers needed for the problem of lifetimes can be computed by the method of the elastic band or string [3,4]. The full computation of the lifetimes requires including thermal noise in the micromagnetic equation of motion (see, e.g., Ref. [5]). In some cases, magnetic systems can be modeled as a single domain (SD) [6]. In a more general case of extended magnetic systems, the system has to be discretized into cells upon which thermal noises are acting. In fact, thermal noises are also acting inside the cells decreasing the magnetization and the exchange stiffness at finite temperatures, also possibly controlling the effective damping constant. Thus, the question of the discretization becomes nontrivial and there were claims that the results of micromagnetic computations at finite temperatures depend on the discretization (see the discussion in Ref. [7]). In addition, the macroscopic magnetization $M(T)$ can dynamically change its magnitude that cannot be described by the Landau-Lifshitz equation [8] and requires using its finite-temperature extension, the Landau-Lifshitz-Bloch (LLB) equation [9,10].

With the increasing of computer power, the atomistic approach considering magnetic materials as a collection of spins on the lattice becomes very promising. Within this framework, one can accurately describe thermal properties such as the heat capacity, temperature dependence of the anisotropy constants, and even phase transitions. For most applications, spins can be considered as classical and obeying the Landau-Lifshitz equation [8] with the Langevin stochastic fields (the LLL equation introduced in magnetism by Brown [11]) mimicking the influence of the thermal bath. The latter lead to thermally activated escape out of metastable states.

Thermal stability of metastable states of single-domain magnetic particles was mainly investigated considering them as single spins [12,13] and using the Fokker-Planck equation. Early numerical work on single spins with the stochastic Landau-Lifshitz-Langevin (LLL) equation was done in Refs. [14,15]. However, there are important many-spin aspects of magnetic nanoparticles, especially related to the surface anisotropy [16,17] (see also Ref. [18] for a review). Nonuniform magnetization via nucleation in magnetic nanoparticles was studied in Ref. [19] by Monte Carlo. Solving the LLL equation for a collection of spins requires much more computing power and is much more difficult [10,20–23].

One of the problems is the stochastic nature of these ordinary differential equations (ODEs) that prevented using high-order solvers such as the classical Runge-Kutta-4 routine. Most of the researchers used the second-order Heun ODE solver [15,23] with a rather short time step. In Ref. [7] it is argued that the mentioned above dependence of the results of thermal micromagnetic computations on the cell discretization was to blame on the limitations of the integration routines, and an implicit Gauss-Seidel method was used to show that the results do not depend on the discretization. However, implicit integration methods, although more stable, require solving large systems of linear equations at each step

and cannot be the most efficient. Another problem is the need of generating stochastic fields for the whole multispin system at every integration step. Although standard random number generators are highly efficient codes, they cannot be much faster than the compiled codes of ODE solvers and thus they essentially contribute to the total computation time.

Recently the pulse-noise approach overcoming these two problems has been proposed [24]. The stochastic fields are represented by rare pulses rotating spins at different angles around different axes, and in the intervals between the pulses high-order ODE solvers with a larger time step can be used. The pulse-noise model is working well in the cases of low and intermediate damping and at low temperatures, where Langevin fields are weak.

In this paper, the pulse-noise approach is applied to uniform thermal activation of single-domain magnetic particles, including a comparison with the single-spin model, and to nonuniform thermal activation via moving domain walls in elongated objects such as magnetic chains. For this purpose, the crossover from uniform to nonuniform thermal escape is studied analytically and formulas for the escape barrier in different cases are worked out. This system was considered in Ref. [25] with the help of Monte Carlo and the LLL equation at high damping. Here the focus is on the much less studied low-damping regime. While computations yield Arrhenius escape rates with correct barriers in most cases, comparison with available theoretical results for the prefactors is much more difficult. In particular, the thermal-activation prefactor for SD particles is by more than order of magnitude higher than that for the equivalent single spins.

It has to be noted that mathematically the pulse-noise approach is close to the jump-noise model proposed in Refs. [26,27] and using the equation of motion of the type $d\mathbf{M}/dt = \cdots + \mathbf{T}(t)$, where $\mathbf{T}$ is a random sequence of finite rotations of $\mathbf{M}$. Whereas the pulse-noise approach is merely a computation tool for solving the standard Landau-Lifshitz-Langevin equation, the jump-noise model is a different stochastic model in magnetism. In the pulse-noise approach, spin rotations have to be small to reproduce the LLL equation. The jump-noise model with small jumps also reproduces the LLL equation. However, jumps can be large as well, leading to a different physics. A detailed comparison of the two approaches is beyond the scope of this paper.

The structure of the main part of the paper is the following. Section II introduces the stochastic model of classical spins, presents known results for thermal activation of single spins, and reviews the pulse-noise method. Section III shows the numerical results for single-domain magnetic particles in comparison with the single-spin model. In Sec. IV analytical results for elongated particles with transverse and longitudinal fields are derived. Section V investigates the dynamics of thermal switching of magnetic chains in different regimes and shows the numerical results for the escape rate $\Gamma(T)$ testing the barrier formulas of the preceding section. In Sec. VI the linear-stability analysis of single-domain barrier states within the chosen model is done. In Sec. VII crossover between uniform and nonuniform thermal activation is studied with the help of the variational method.

II. THE MODEL AND THE METHODS

Consider a parallelepiped-shape magnetic particle with a simple cubic lattice described by the classical-spin Hamiltonian

$$\mathcal{H} = \sum_i \left(-Ds_{zi}^2 + D_y s_{yi}^2 \right) - \mu_0 \mathbf{H} \sum_i \mathbf{s}_i - \frac{1}{2} \sum_{ij} J_{ij} \mathbf{s}_i \cdot \mathbf{s}_j, \tag{1}$$

where $|\mathbf{s}_i| = 1$, $\mathbf{H}$ is the magnetic field, μ_0 is the magnetic moment of the atom, J_{ij} is the exchange with J being the nearest-neighbor exchange coupling, $D > 0$ is the uniaxial-anisotropy constant, and $D_y > 0$ is the hard-axis y anisotropy. One can also include a surface anisotropy and the dipole-dipole interaction. The latter, for single-domain particles, gives rise to the biaxial anisotropy, $D_y > 0$, if the particle has a shape flat in the y direction.

The dynamics is described by the Landau-Lifshitz-Langevin (LLL) equation

$$\dot{\mathbf{s}}_i = \gamma [\mathbf{s}_i \times (\mathbf{H}_{\text{eff},i} + \boldsymbol{\zeta}_i)] - \gamma\lambda [\mathbf{s}_i \times [\mathbf{s}_i \times \mathbf{H}_{\text{eff},i}]], \tag{2}$$

where $\mathbf{H}_{\text{eff},i} \equiv -\partial\mathcal{H}/\partial\mathbf{s}_i$ is the effective field,

$$\mu_0 \mathbf{H}_{\text{eff},i} = \mu_0 \mathbf{H} + 2Ds_{zi}\mathbf{e}_z - 2D_y s_{yi}\mathbf{e}_y + \sum_j J_{ij}\mathbf{s}_j, \tag{3}$$

γ is the gyromagnetic ratio, λ is the dimensionless damping constant [8], and $\boldsymbol{\zeta}_i$ are stochastic fields. Landau and Lifshitz have written the double-vector-product relaxation term on general grounds. Later it was demonstrated that the vector product in the noise term dictates the double-vector product form of the damping term [28]. The stochastic model above is equivalent to the Fokker-Planck equation introduced by Brown for superparamagnetic particles [11] (see also Ref. [29]). The equilibrium solution of the Fokker-Planck equation should be a Boltzmann distribution, that requires a relation between damping and noise,

$$\langle \zeta_{\alpha,i}(t)\zeta_{\beta,j}(t') \rangle = \frac{2\lambda T}{\gamma\mu_0} \delta_{ij}\delta_{\alpha\beta}\delta(t-t'), \tag{4}$$

where $k_B = 1$ is set. Microscopic theories suggest $\lambda \ll 1$. In the case of spin magnetism with one type of magnetic atoms, one has $\mu_0 = g\mu_B S$, where $g = 2$, μ_B is Bohr's magneton, S is the spin value of the magnetic atom, and γ is given by $\gamma = g\mu_B/\hbar$, so that $\gamma\mu_0 = (g\mu_B)^2 S/\hbar$.

In computations, J and most other parameters and physical constants are set to 1, so that one needs a relation between the time t in computations and the real time t_{real}. For the original system the exchange frequency is $\omega_{ex} = SJ/\hbar$. As this frequency is set to 1, the relation between the times reads $t_{\text{real}} = \frac{\hbar}{SJ} t$. For metallic Co, $J = 93$ K and $S = 3/2$, so that $t_{\text{real}} = 5.3 \times 10^{-14} t$ s. The maximal computation time in the present work $t = 10^6$ corresponds to $t_{\text{real}} = 5.3 \times 10^{-8}$ s or 53 ns for Co. It is clear that computations cannot be extended to seconds and extrapolation of the computational results is needed. Further, the uniaxial anisotropy of Co is 0.22 K per atom; thus in J units one has $D = 0.22/96 = 0.0023$. Pt alloys CoPt and FePt have a comparable exchange but a much stronger anisotropy: $D = 4.1/96 = 0.044$ for CoPt and $D = 5.7/105 = 0.054$ for FePt.

Uniaxial anisotropy creates an energy barrier U between spin directions parallel and antiparallel to z axis. If the particle is in the single-domain (SD) state, which is realized for not too large sizes, then in the absence of the field the barrier is given by $U = U_{SD} \equiv \mathcal{N}D$, where $\mathcal{N} \equiv N_x N_y N_z$ is the number of spins in the particle. Applied field lowers the barrier. The barrier exists within the Stoner-Wohlfarth astroid [30,31],

$$h_x^{2/3} + h_z^{2/3} \leqslant 1, \quad h_x \equiv \frac{\mu_0 H_x}{2D}, \quad h_z \equiv \frac{\mu_0 H_z}{2D}. \tag{5}$$

There are formulas for the barrier in the cases of purely transverse and purely longitudinal field [32],

$$U_{SD} = \mathcal{N}D(1 - h_x)^2, \quad U_{SD} = \mathcal{N}D(1 - h_z)^2. \tag{6}$$

For particle of a larger size, the barrier state becomes nonuniform and for elongated particles it corresponds to a domain wall bisecting the particle. In zero field, the nonuniform barrier is the energy of a domain wall (DW) given by [8]

$$U_{DW} = \mathcal{N}D\frac{4\delta}{L_z} = \frac{4\delta}{a}N_x N_y D, \quad \delta = a\sqrt{\frac{J}{2D}}, \tag{7}$$

where δ is the domain-wall width, a is the lattice spacing, and $L_z \equiv aN_z$ is the longest particle's dimension. The particle is overcoming the barrier in the single-domain state if $U_{SD} < U_{DW}$ that amounts to $L_z \lesssim \delta$. The numerical coefficient in this formula has to be worked out, including the cases with the field applied.

At low temperatures, $T \ll U$, the particle is overcoming the barrier via thermal activation that yields the escape rate of the Arrhenius form

$$\Gamma = \Gamma_0 e^{-U/T}. \tag{8}$$

The process is described by Eq. (2) or the equivalent Fokker-Planck equation. The latter is suitable for the analytical work, especially in the SD regime, and it allows one to obtain the formula above with different expressions for the prefactor Γ_0 in different parameter regions. For a single spin, in the axially symmetric case $\Gamma_0 \propto \lambda$. If there is a saddle of the spin's energy (created by the transverse field or transverse anisotropy), then there are three regimes of strong, intermediate, and low damping. In the strong-damping case, $\Gamma_0 \propto \lambda$, if the Landau-Lifshitz equation is used. In the intermediate-damping case Γ_0 is independent of λ which corresponds to the transition-state theory. However, this regime is realized in a pretty narrow region of λ. In the low-damping case $\Gamma_0 \propto \lambda$ again. There are numerous crossovers between these three regimes and the uniaxial regime [33]. Analytical solution of the multidimensional Fokker-Planck equation for nonuniform thermal activation is a challenging task. First, the barrier has to be found as the saddle point of the particle's energy in a nonuniform state (see, e.g., [34,35]). The corresponding analytical results will be summarized below. Second, calculation of the prefactor in Eq. (8) requires application of functional methods and is especially nontrivial [36].

Numerically, the Fokker-Planck equation can be solved by the matrix-continued-fraction method [13,37] that is very fast and accurate. However, setting up equations for different kinds of anisotropy requires serious work. For many-spin systems this method becomes unusable.

The most straightforward method of numerically solving the problem of thermal activation (apart of the time-quantified Monte Carlo [38,39]) is using Eq. (2). The particle is prepared in a collinear state corresponding to one of the energy minima, then Eq. (2) is solved until the particle crosses the barrier. This yields the first-passage time for a given computation. Such computations can be run in parallel, and the inverse of the mean first-passage time is identified with the escape rate Γ. In fact, there is a more efficient method of data processing described in the Appendix.

At low temperatures where Γ is exponentially small, the computations leading to particle's escape are very long. Usually the second-order Heun method with a rather short time step is used to integrate the stochastic LLL equation. For this reason, the LLL equation was mainly solved for single-domain thermal activation considering the magnetic particle as a single spin.

It was recently shown [24] that in the relevant regions of intermediate and low damping the continuous noise can be replaced by a pulse noise with time interval Δt that has to satisfy the two conditions

$$\Lambda_N \Delta t \ll 1, \quad \gamma\lambda H_{\text{eff}} \Delta t \ll 1, \tag{9}$$

where $\Lambda_N \equiv 2\gamma\lambda T/\mu_0$ is the so-called Néel attempt frequency, i.e., the high-temperature relaxation rate. The pulse consists in rotating spins by the angles

$$\boldsymbol{\varphi}_i = \sqrt{\Lambda_N \Delta t}\,\mathbf{G}_i, \tag{10}$$

where $\mathbf{G}_i$ is a realization of a three-component vector, each component being a normal distribution with a unit dispersion. In the interval between the pulses, high-order numerical integrators (for instance, the classical RK4 or Butcher's RK5; see, e.g., the Appendix of Ref. [24]) for the damped equations without noise can be used. The step δt of the numerical integration can be chosen much greater than that used with the Heun method, which gives a considerable speedup. At low damping λ, one can choose $\delta t \ll \Delta t$ which makes the contribution of the random-number generation into the computation time negligible. Thus the speed of the method becomes the same as the speed of noiseless computations. This allows one to numerically solve the problem of thermal activation of magnetic particles within the many-spin model, including the case of nonuniform thermal activation. The lower the temperature (that is, the smaller is the noise) and the damping λ, the better the applicability conditions of Eq. (9) are satisfied. In the sequel, some of such problems will be considered.

Typically, numerical solutions used $\Delta t = 1$ and $\delta t = 0.1$ with Butcher's RK5 ODE solver. Such parameters, with $J = 1$, ensure a good numerical accuracy [24]. It should be noted that although at low temperatures the dynamics is governed by D and H that define the precession frequency of the particle, the required integration step δt is dictated by the exchange J. If $J\delta t \ll 1$ is not satisfied, explicit integrators used here show instabilities. The latter usually happen for $J\delta t > 0.25$. The physical reason is that for large J increasing the spin noncollinearity with the neighbors leads to a very fast precession that a large-step integrator cannot handle. This aspect is absent in the one-spin models of magnetic particles and it makes a problem for a small ratio D/J.

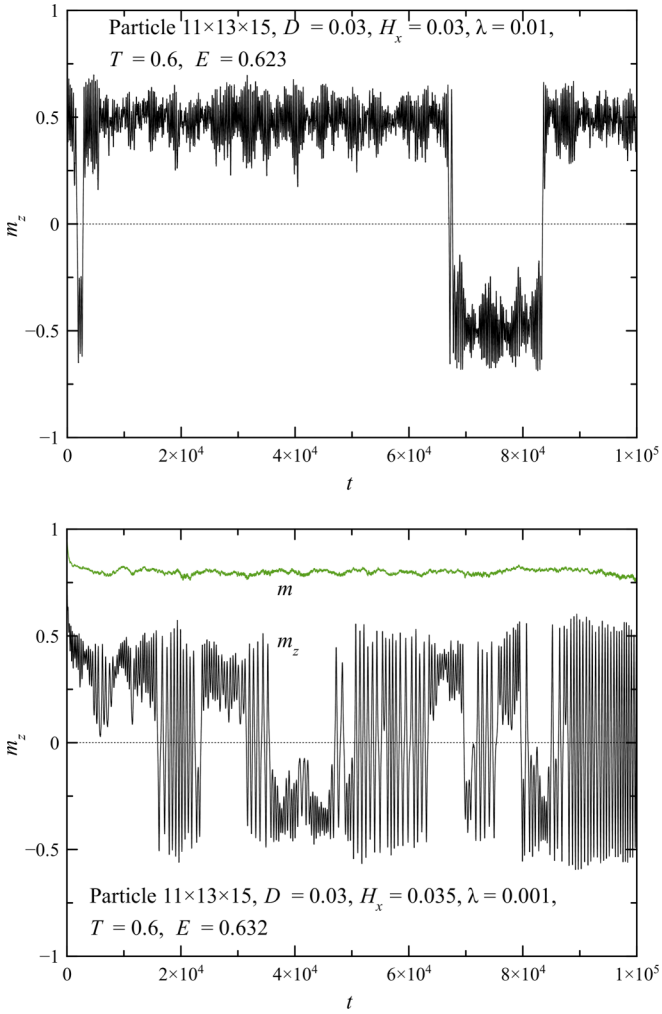

FIG. 1. Thermal switching dynamics of a single-domain particle with transverse field at elevated temperature $T = 0.6$ for different values of the damping λ. Upper panel: $\lambda = 0.01$. Lower panel: $\lambda = 0.001$ (energy diffusion regime).

The main computer used in these computations was a Dell Precision T7610 workstation with two dual Intel Xeon processors E5-2680, each having 10 cores. The algorithm was implemented within Wolfram Mathematica with compilation and parallelization. In computations, the energy was measured in the J units, that is, J was set to 1, together with μ_0, γ, and the lattice spacing a. The bulk of computations was performed on particles with free boundary conditions.

III. THERMAL SWITCHING OF SINGLE-DOMAIN MAGNETIC PARTICLES

In this section, thermal activation of particles in the single-domain regime is studied. Figure 1 shows the activation dynamics and transitions between the energy minima for a $11 \times 13 \times 15$ particle containing 2145 spins with $D = 0.03$ and transverse field at $T = 0.6$ that is not small in comparison with the bulk Curie temperature $T_C = 1.444J$ of the classical 3D Heisenberg model. In the upper panel, the results for the particle with $H_x = 0.03$ and $\lambda = 0.01$, prepared in the collinear state in the energy minimum at $\theta = \arcsin h_x = 30^\circ$ to the z axis, show robust jumps between the energy minima characteristic of strong-to-intermediate damping. The magnitude m of the particle's magnetization

$$\mathbf{m} \equiv \frac{1}{\mathcal{N}} \sum_i \mathbf{s}_i \tag{11}$$

demonstrates a considerable thermal disordering that one can see from the value $m \approx 0.8$ in the lower panel. The average energy of the system E, with respect to that of the fully ordered state, is close to T. In the lower panel, dynamics of the particle with $\lambda = 0.001$ is clearly underdamped. This is the energy-diffusion regime, in which, as the particle acquires an energy above the barrier, it begins crossing it repeatedly. m is not changing essentially during crossing the barrier in the above computations; thus one can conclude that the particle remains in the single-domain state.

Single-domain particles are usually thought of as effective single spins. Of course, the single-spin model (SSM) is much easier for computations than the original many-spin model. The corresponding mapping can be obtained by setting up the equation of motion for $\mathbf{m}$ of Eq. (11) using Eq. (2) for tightly bound spins. The result has the same form as the latter, however, with the global Langevin field

$$\boldsymbol{\Xi} = \frac{1}{\mathcal{N}} \sum_i \boldsymbol{\zeta}_i \tag{12}$$

whose correlators are given by

$$\langle \Xi_\alpha(t) \Xi_\beta(t') \rangle = \frac{2\lambda T}{\gamma \mu_0 \mathcal{N}} \delta_{\alpha\beta} \delta(t - t'). \tag{13}$$

Thus one can map the SD particle onto the single spin by introducing the scaled temperature for the SSM

$$T_{\mathrm{SSM}} = T/\mathcal{N}. \tag{14}$$

As the results for the single spin at the temperature T_{SSM} are expected be the same as the results for the SD particle at T, one can plot the single-spin results obtained at the temperature T_{SSM} vs $T = \mathcal{N} T_{\mathrm{SSM}}$ to compare with those for the SD particle at T.

To systematically study the temperature dependence of the thermal activation rate in the SD regime, a $5 \times 6 \times 7$ particle containing 210 spins was used. Here, again, $D = H_x = 0.03$ which corresponds to $h_x = 1/2$. The barrier value given by Eq. (6) is $U = 210 \times 0.03 \times 0.25 = 1.575$. Crossing the barrier was detected as the change of the sign of the total magnetization projection m_z. The results for three different values $\lambda = 0.1$, 0.01, and 0.001 are shown in the upper panel of Fig. 2. For $T \lesssim 0.2$ that corresponds to $U/T \gtrsim 8$; the escape rate follows the predicted Arrhenius behavior with the barrier value given above.

The lower panel of Fig. 2 shows the escape rates $\Gamma(T)$ for the $5 \times 6 \times 7$ particle with free boundary conditions (the regular case), periodic boundary conditions, and for the equivalent single-spin model. Although the slope of all three curves is the same which indicates the same barrier, the prefactors are essentially different: the highest prefactor for the particle with free boundary conditions and the lowest one for the equivalent single spin.

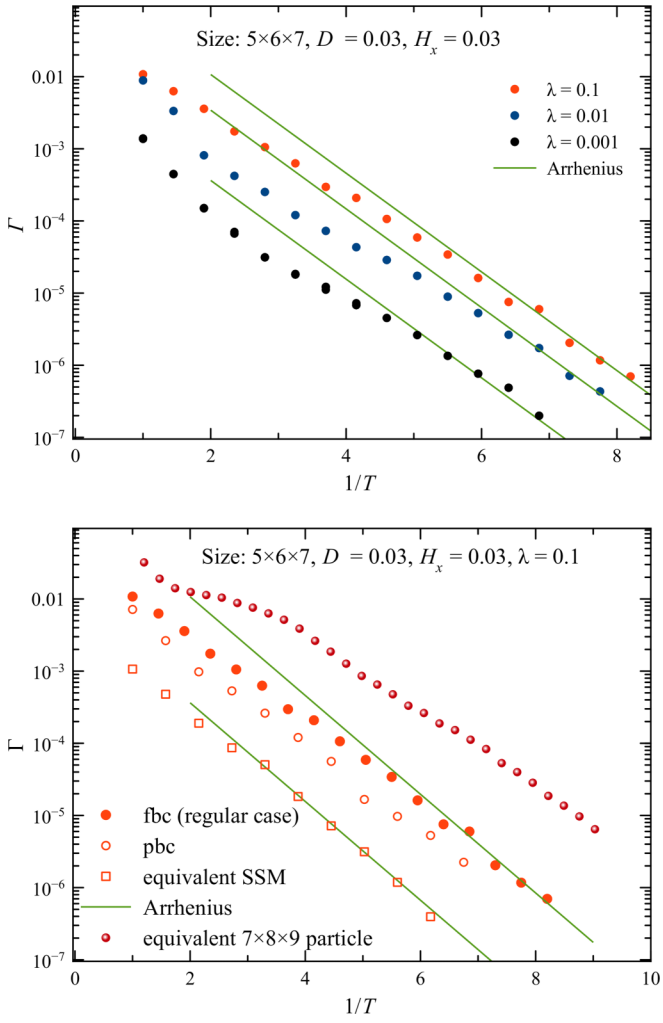

FIG. 2. Thermal escape rate for the $5 \times 6 \times 7$ particle with $D = H_x = 0.03$. Upper panel: Different values of the damping constant $\lambda = 0.1$, 0.01, and 0.001. Lower panel: Systems with free and periodic boundary conditions, compared with the results for an equivalent single spin and for the equivalent $7 \times 8 \times 9$ particle.

In the figure also are shown the results for the larger $7 \times 8 \times 9$ particle containing 504 spins. The temperature for this particle in the plot is scaled in the same way; i.e., the results are plotted vs the scaled temperature $T = (210/504)T_{7\times8\times9}$, where $T_{7\times8\times9}$ is the actual temperature of computations for this model. One can see that here the deviation from the SSM is even more pronounced: the prefactor is much larger and even the barrier is noticeably lower.

The effect of higher thermal escape rates for a many-spin particle was observed earlier [25] and attributed to thermal disordering of the particle. Indeed, the temperature dependence of the magnetization $m(T)$ for classical spin systems at low temperatures is linear: $m(T) \cong 1 - cT/J$. Here the coefficient c depends on the particle's size and on the boundary conditions at the surface [40]. For free boundary conditions there is an additional thermal disordering at the surface, so that c is higher than for the model with periodic boundary conditions. For the SSM this effect is absent, $c = 0$. For the magnetic particle, the barrier acquires a linear temperature dependence via the effective temperature-dependent anisotropy constant [41]. For classical models at low temperatures this dependence has the form

$$U(T) \cong U_0 - bT, \quad b \sim \mathcal{N}Dc/J. \tag{15}$$

As the result, the prefactor in Eq. (8) increases by the factor $\exp(b)$ that can be large, as is the case here. The lower apparent barrier for the $7 \times 8 \times 9$ particle must be a consequence of the higher temperature $T_{7\times8\times9}$ for which the magnetization decreases stronger than linearly. To summarize, the mapping of the SD magnetic particle on the single-spin model is incomplete, as the assumption of tightly bound spins misses the important effect of thermal disordering of the particle.

In quantum mechanics, there is the Bloch law for the magnetization at low temperatures, $m(T) = 1 - c'(T/J)^{3/2}$ and thus $U(T) = U_0 - b'T^{3/2}$ with $b' \sim \mathcal{N}Dc'/J^{3/2}$. In this case the additional temperature-dependent prefactor $\exp(b'\sqrt{T})$ should emerge. At the moment, however, it is unclear how to compute the thermally activated dynamics of quantum spins from first principles.

One can take into account the dynamics of the particle's magnetization at elevated temperatures within the single-spin approach by using the Landau-Lifshitz-Bloch (LLB) equation [9] with added longitudinal stochastic terms changing m [42,43]. Overcoming the barrier, the particle decreases its magnetization, up to its compete disappearance in the barrier state at temperatures close to the Curie temperature [44,45]. This should essentially change the particle's dynamics and thus the thermal-activation prefactor. Note a similar phenomena in the physics of domain walls: in the temperature interval below the Curie temperature the structure of the DW changes so that there is only the z component of the magnetization that changes its sign going through zero [46] and changing the domain-wall dynamics completely [47,48].

In fact, these phenomena can be observed in the present computations on the many-spin model for strong anisotropy and high temperature. Figure 3 shows thermal switching dynamics of a $4 \times 5 \times 6$ particle of 120 spins with biaxial anisotropy $D = D_x = 1$ at a high temperature, $T = 1.5$. In the upper panel, $\lambda = 0.001$, first the particle thermalizes starting from the collinear initial state that takes some time because of the low damping, then it begins to jump between the energy minima. One can see that m_z correlates with m and that m turns to zero when m_z changes its sign. In the lower panel, the computation was continued setting $\lambda = 0$. The results clearly show that the particle can cross the barrier even without a coupling to the bath. The reason is that the magnetic particle has internal degrees of freedom, spin waves, that can serve as the particle's own bath. The contribution from internal spin waves enters the precessional equation of motion for the particle's magnetization, Eq. (21) of Ref. [49], and it could play the role of thermal noise helping to surmount the barrier. It is interesting that switching off the damping increased the rate of over-barrier transitions. Although the dynamics is conservative, the results look incoherent which is a consequence of a strong thermal spin disordering in the cluster. Since the directions of neighboring spins strongly deviate at such high temperature, it is difficult to decide whether the magnetization switching is uniform or not, especially in small clusters.

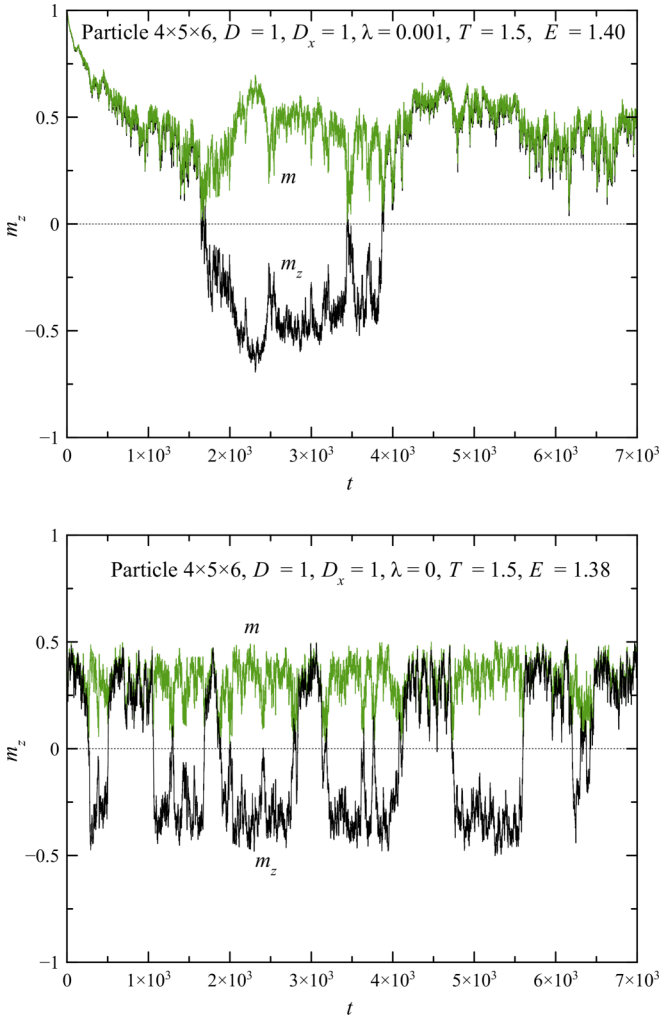

FIG. 3. Thermal switching via changing the magnetization m of a $4 \times 5 \times 6$ particle with biaxial anisotropy $D = D_x = 1$ at high temperature, $T = 1.5$. Upper panel: $\lambda = 0.001$. Lower panel: $\lambda = 0$.

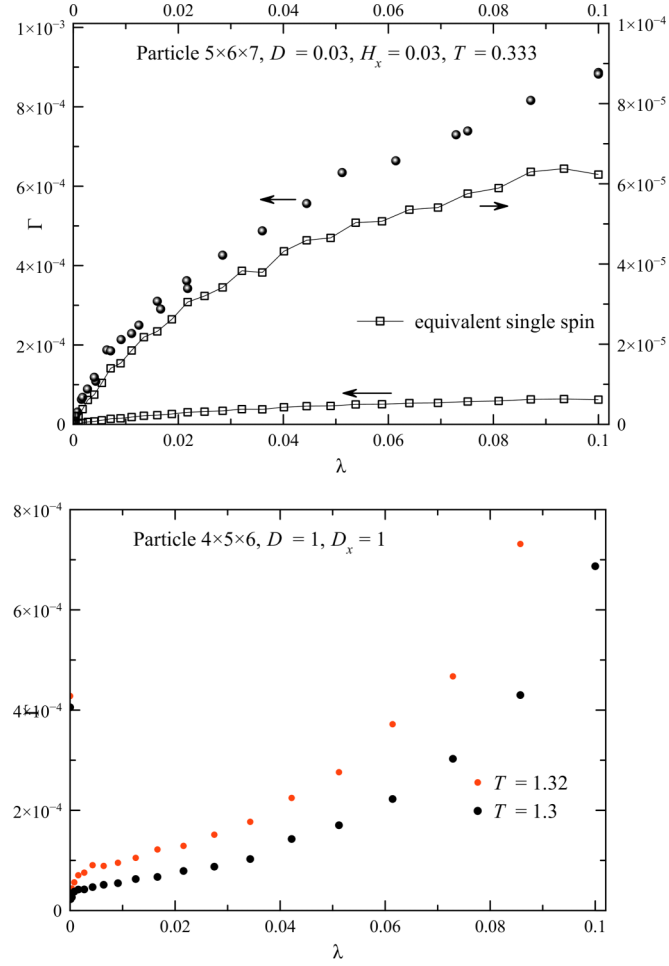

FIG. 4. Thermal escape rate vs λ. Upper panel: $5 \times 6 \times 7$ particle with $D = H_x = 0.03$ at $T = 0.333$, compared with the result for the equivalent single spin. For the latter, the escape rate is by more than an order of magnitude lower. Lower panel: $4 \times 5 \times 6$ particle with $D = D_x = 1$ at $T = 1.3$. Thermal switching via longitudinal relaxation, even in the absence of the coupling to the external bath.

The λ dependence of the escape rate in the upper panel of Fig. 4 shows mainly the low-damping regime with a beginning of a crossover to the intermediate-damping regime at largest λ. Escape rate vanishing at $\lambda \to 0$ is expected for a single spin. However, for a particle this is nontrivial since the particle has its own internal bath [49]. The likely reason is that the contribution of the internal spin waves is quadratic in the anisotropy that does not break the translational invariance [49], such as the volume anisotropy in Eq. (1), so that the effect of the internal bath is weak for small anisotropies and low temperatures. For strong anisotropy and high temperature, escape via the internal bath at $\lambda = 0$ is possible, as can be seen in the lower panel of Fig. 4. The inverted curvature of the λ dependence of the switching rate indicates a different type of dynamics, likely the longitudinal relaxation.

It should be noted that these computations start from the collinear spin state and it requires a warming time to reach the preset temperature T. In the limit $\lambda \to 0$, the warming time goes to infinity; this is why Γ vanishes at the smallest λ in the lower panel of Fig. 4. To study thermal switching at $\lambda = 0$, pre-warming is needed, as in the lower panel of Fig. 3.

IV. NONUNIFORM ENERGY BARRIERS FOR LONG PARTICLES

As said above, there are many different limits for the thermal activation prefactor Γ_0, especially for the nonuniform thermal activation. Thus here the analytical attention will be given to the barrier U, while prefactors can be determined numerically.

To find the nonuniform barrier, one needs the continuous approximation for the particle's energy, Eq. (1),

$$\mathcal{H} = \frac{1}{a^3}\int dV \left\{ \frac{1}{2}a^2 J \left(\frac{\partial s_\alpha}{\partial \mathbf{r}} \right)^2 - D s_z^2 + D_y s_y^2 - \mu_0 \mathbf{H} \cdot \mathbf{s} \right\} \tag{16}$$

with summation over the repeated α. Minimizing this energy leads to the equation

$$\mathbf{s}\times(\mu_0\mathbf{H}+2Ds_z\mathbf{e}_z-2D_ys_y\mathbf{e}_y+a^2J\Delta\mathbf{s})=0 \tag{17}$$

with the boundary condition

$$\mathbf{s}\times\frac{\partial\mathbf{s}}{\partial r_\alpha}n_\alpha=0 \tag{18}$$

at the surfaces, where $\mathbf{n}$ is the normal to the surface.

We will consider a particle elongated along the z axis and search for the solution in the form $\mathbf{s}=(s_x(z),0,s_z(z))$, also assuming $\mathbf{H}=(H_x,0,H_z)$. Then only the y component of Eq. (17) is nonzero. In terms of the parameters introduced in Eqs. (5) and (7), one has

$$s_z(h_x+\delta^2s_x'')-s_x(h_z+s_z+\delta^2s_z'')=0, \tag{19}$$

while the boundary condition becomes $s_x'=s_z'=0$. The energy, Eq. (16), in this case becomes

$$E=\frac{\mathcal{N}D}{L_z}\int_0^{L_z}dz\{\delta^2[(s_x')^2+(s_z')^2]+1-s_z^2-2\mathbf{h}\cdot\mathbf{s}\}. \tag{20}$$

In the transverse field, $h_x>0$, the solution for the domain-wall profile in the infinite system has the form

$$s_z=\pm\sqrt{1-h_x^2}\,\frac{\sinh\frac{z-z_0}{\delta_h}}{h_x+\cosh\frac{z-z_0}{\delta_h}},\quad s_x=\frac{1+h_x\cosh\frac{z-z_0}{\delta_h}}{h_x+\cosh\frac{z-z_0}{\delta_h}}, \tag{21}$$

where $\delta_h\equiv\delta/\sqrt{1-h_x^2}$ [50]. The barrier state corresponds to the DW in the center of the particle, $z_0=L_z/2$. For $L_z\gg\delta$, the boundary conditions at the ends are practically satisfied, and one can use this solution to calculate the barrier energy using Eq. (20) with $h_z=0$. The result has the form

$$U_{DW}(h_x)=4\mathcal{N}D\frac{\delta}{L_z}\left(\sqrt{1-h_x^2}-2h_x\arctan\sqrt{\frac{1-h_x}{1+h_x}}\right). \tag{22}$$

The limiting cases of this formula are

$$\frac{U_{DW}(h_x)}{U_{DW}(0)}\cong\begin{cases}1-\frac{\pi}{2}h_x, & h_x\ll1,\\ \frac{2^{3/2}}{3}(1-h_x)^{3/2}, & 1-h_x\ll1.\end{cases} \tag{23}$$

In the longitudinal field, $h_z>0$, one can use the saddle-point solution found for the infinite system [34], in our case centered at one of the particle's ends, say, near $z=0$,

$$\tan\frac{\theta}{2}=\sqrt{\frac{h_z}{1-h_z}}\cosh\left(\frac{\sqrt{1-h_z}}{\delta}z\right). \tag{24}$$

Centering the solution at the particle's end reduces the barrier by a factor of two in comparison to centering in the middle of the particle. The spin components are given by

$$s_z=\frac{1-\tan^2(\theta/2)}{1+\tan^2(\theta/2)},\quad s_x=\frac{2\tan(\theta/2)}{1+\tan^2(\theta/2)}, \tag{25}$$

where the sign in front of s_z is chosen so that $s_z=-1$ ($\theta=\pi$) at infinity (the metastable state for $h_z>0$). This solution satisfies Eq. (19) with $h_x=0$ and the boundary conditions.

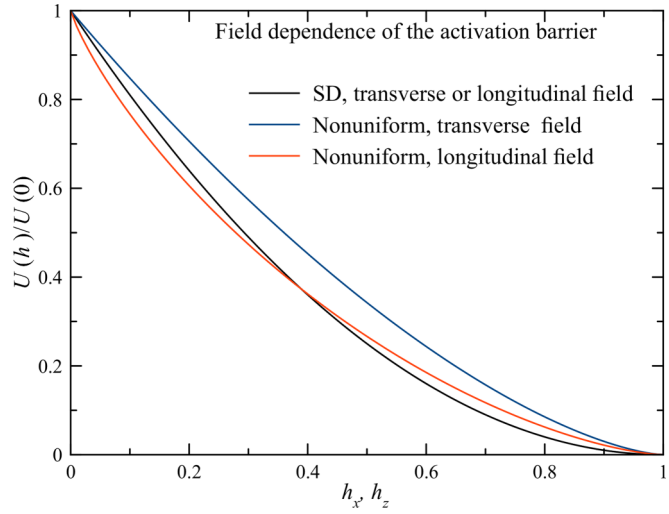

FIG. 5. Field dependence of the energy barrier for magnetic particles in the uniform (SD) and nonuniform regimes.

One has $s_z(0)=1-2h_z$. For $h_z\ll1$ this yields $s_z(0)\cong1$, whereas the point at which $s_z=0$ ($\theta=\pi/2$) is far from the end of the particle. This is a domain wall in the particle's bulk. For $1-h_z\ll1$ one has $s_z(0)\cong-1$ which is a very small deviation from the metastable state.

The energy barrier is equal to the difference of the barrier energy and the energy of the metastable state $\propto 2h_z$. Equation (20) with $h_x=0$ yields

$$U(h_z)=4\mathcal{N}D\frac{\delta}{L_z}\left[\sqrt{1-h_z}-\frac{h_z}{2}\ln\frac{1+\sqrt{1-h_z}}{1-\sqrt{1-h_z}}\right]. \tag{26}$$

The limits of this formula are

$$\frac{U(h_z)}{U_{DW}(0)}=\begin{cases}1-\frac{h_z}{2}\left(1+\ln\frac{4}{h_z}\right), & h_z\ll1,\\ \frac{2}{3}(1-h_z)^{3/2}, & 1-h_z\ll1.\end{cases} \tag{27}$$

Fields dependencies of the barrier worked out above, as well as Eq. (6) for the SD particle, are shown in Fig. 5.

V. THERMAL SWITCHING OF SPIN CHAINS

The simplest realization of elongated particles is spin chains. A chain of $L=100$ particles with $D=0.01$ has the DW width $\delta\simeq7\ll L$ and is expected to overcome the barriers at low temperatures via a moving domain wall. The results for thermal switching dynamics for this chain in the transverse field $H_x=0.01$ at $T=0.015$ and 0.025 for the intermediate and low damping λ, shown in Fig. 6, are similar to those for the single-domain particle in Fig. 1. The magnetization magnitude m decreases when the chain is crossing the barrier ($m_z=0$) but this decrease is much less than 50%, so that the barrier state of the chain is closer to a single-domain state than to a state with a moving domain wall that would result in $m=0$ when the DW is in the chain's center. Spin configurations corresponding to crossing the barrier show spins nearly perpendicular to the z axis with noticeable disordering due to thermal spin waves. Observation of thermal activation via a moving domain wall in this case requires lowering the temperature.

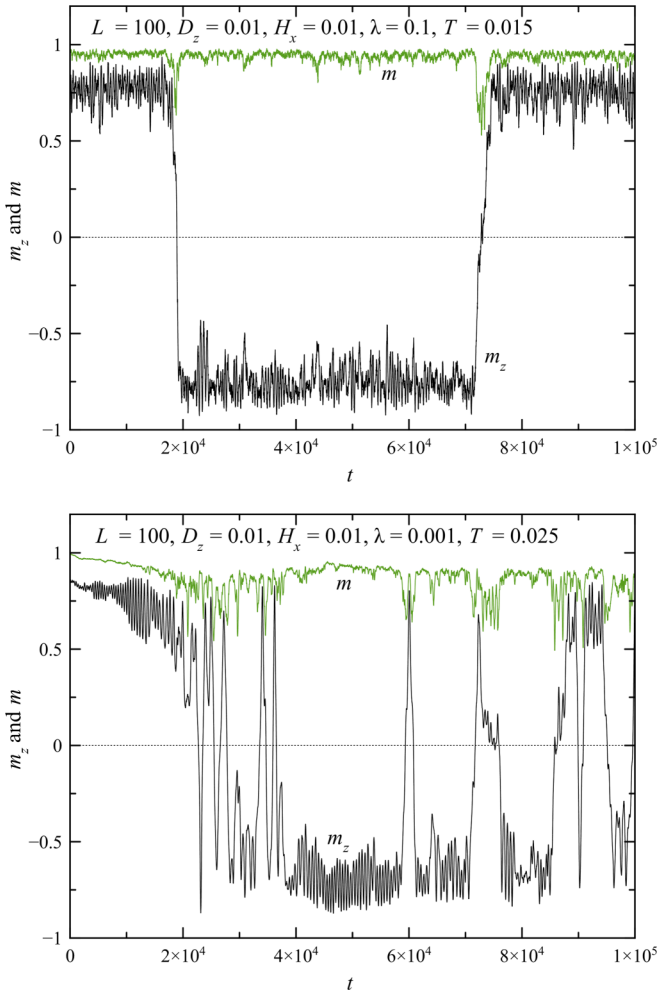

FIG. 6. Thermal switching dynamics of a magnetic chain of 100 spins with transverse field for different values of the damping λ. Upper panel: $\lambda = 0.01$. Lower panel: $\lambda = 0.001$ (energy diffusion regime). Unlike the SD particle in Fig. 1, here domain walls are traversing the chain in different directions, changing the sign of m_z.

Field-biased chains show more affinity to crossing the barrier via moving domain walls. Thermal switching dynamics of a 100-spin chain with $D = 0.01$ and $H_z = -0.015$ in Fig. 7 shows a significant reduction of m on barrier crossing. After emerging at one of the chain's ends, the DW is pushed to the other end by the bias field H_z. In the axially symmetric case, domain walls can move only via the damping with the mobility $v/H_z \propto \lambda$, so that for $\lambda = 0.01$ their speed v is low, as can be seen on the right side of Fig. 7. During this slow motion, the spins in the DW are precessing around the z axis.

Adding the hard-axis y anisotropy D_y breaks the axial invariance and allows the domain wall to travel with the mobility $v/H_z \propto 1/\lambda$, if the applied field is not too strong. In this regime, its speed is limited by the Walker velocity $v_W \propto D_y$. In Fig. 7 one can see a fast switching in the chain with $D_y = 0.01$. Decreasing λ to 0.001 does not change the slope of m_z for the biaxial spin chain; thus one can conclude that the motion of domain walls here is ballistic. This ballistic motion can become unstable as shown in Fig. 8 which leads to precession of spins around the z axis (vertical axis in this

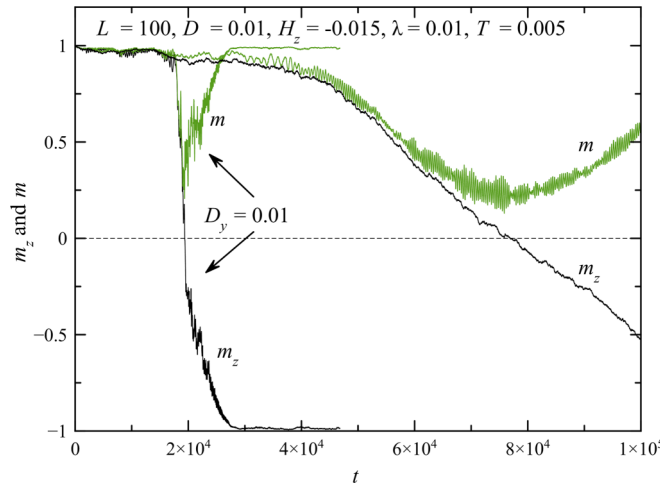

FIG. 7. Thermal switching of a field-biased magnetic chain of 100 spins occurs via moving domain walls as the magnetization m strongly decreases in the process. Adding the hard-axis y anisotropy D_y speeds up the motion of the domain wall.

figure) and slowing down the DW motion. This typically causes formation of solitons (360° domain walls) captured inside the chain, seen in the lower panel of Fig. 8, which take some time to exit through the ends. The dynamics of a chain of a finite length L_z becomes more complicated because of the boundary conditions at the ends which influence the domain walls and cause reflection of spin waves. The initial moment of reversal seen in the second, third, and fourth rows looks like a high-amplitude spin wave turning spins on the left perpendicular to the easy axis rather than like a nascent domain wall.

Computations of the temperature dependence of the thermal activation rates were performed on the 50-spin chain with $D = 0.01$ and the damping values $\lambda = 0.1, 0.01$, and 0.001. In the axially symmetric case shown in the upper panel of Fig. 9 the Arrhenius regime with the nonuniform barrier given by Eq. (7) sets in at low temperatures. The prefactor Γ_0 is clearly proportional to λ, as it is for single-domain particles in this case. Data for the 100-spin chain show a slower escape with an apparent barrier slightly higher at low temperatures. This can indicate an increasing contribution of the nucleation via a couple of opposite domain walls inside the chain for which the barrier is twice as large

The data in the case of a strong transverse field in the lower panel of Fig. 9 align with the Arrhenius dependence with the barrier given by Eq. (22), the energy of a domain wall with transverse field. However, this happens at rather low temperatures, especially in the low-damping case. This should not be a surprise as the dynamics of domain walls crossing the barrier is rather complicated, as we have seen above.

Videos of thermal switching of spin chains in different regimes considered above can be found in the Supplemental Material [51].

VI. LINEAR INSTABILITY OF THE UNIFORM BARRIER STATE

Let us investigate the stability of the single-domain barrier state with spins directed along $\mathbf{e}_b$, the barrier direction in the

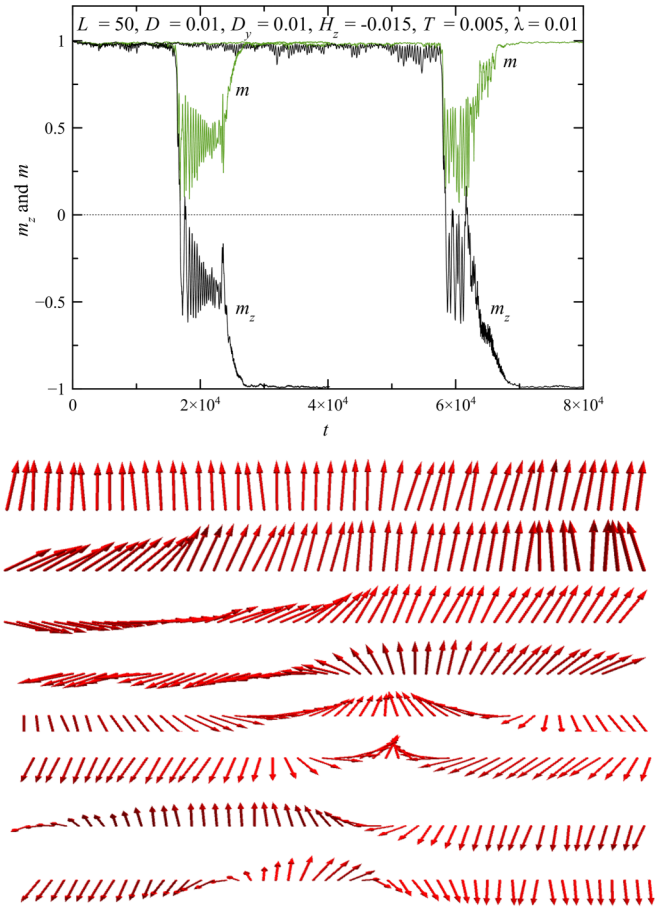

FIG. 8. Two realizations of thermal switching of a field-biased biaxial magnetic chain of 50 spins with fast and unstable domain-wall motion. Upper panel: Time dependence of the magnetization. Lower panel: Spin configurations at different moments of switching for the second realization. (Easy axis vertical.)

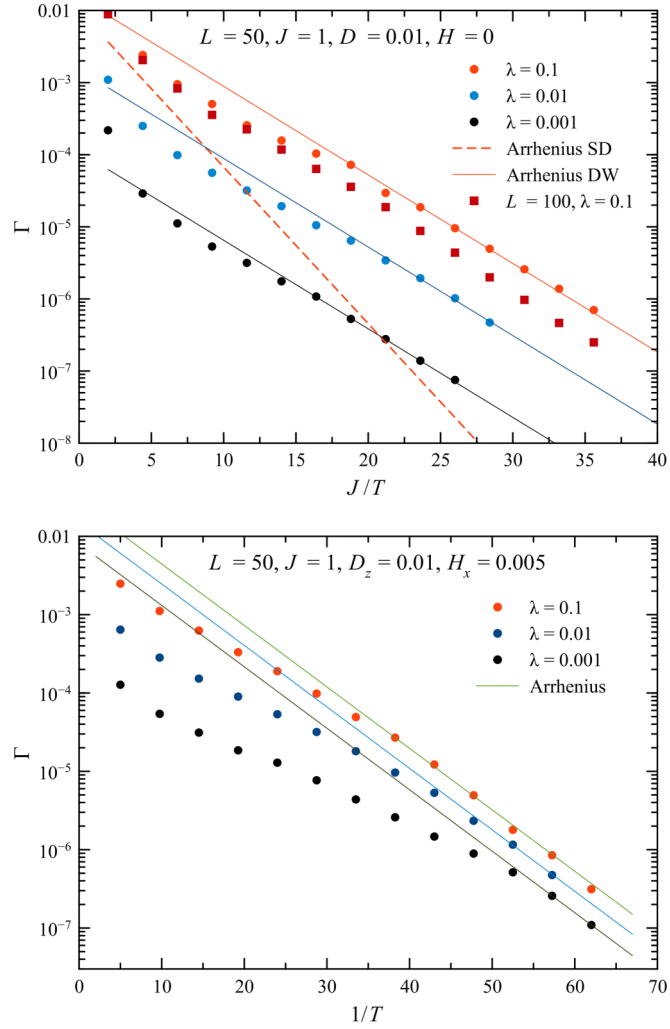

FIG. 9. Thermal escape rate for the 50-spin chain with $D = 0.01$ and $\lambda = 0.1$, 0.01, and 0.001. Upper panel: Zero field. Results for the 100-spin chain with $\lambda = 0.1$ added for a comparison. Lower panel: $H_x = 0.05$. For $\lambda = 0.001$, the asymptotic behavior is realized only at very low temperatures.

xz plane. Taking into account nonuniform deviations from the barrier direction, the spins can be represented as

$$\mathbf{s} = \mathbf{e}_b\sqrt{1-\psi^2} + \mathbf{e}_{b'}\psi \cong \mathbf{e}_b\left(1 - \frac{1}{2}\psi^2\right) + \mathbf{e}_{b'}\psi, \qquad (28)$$

where $\mathbf{e}_{b'}$ is in the xz plane perpendicular to $\mathbf{e}_b$. Substituting this into Eq. (20), one obtains the nonuniform energy up to ψ^2:

$$\delta E = \frac{\mathcal{N}D}{L_z}\int_0^{L_z} dz\{\delta^2\psi'^2 - 2A\psi - B\psi^2\}, \qquad (29)$$

where

$$A \equiv (\mathbf{e}_z\cdot\mathbf{e}_b)(\mathbf{e}_z\cdot\mathbf{e}_{b'}) + \mathbf{h}\cdot\mathbf{e}_{b'},$$
$$B \equiv (\mathbf{e}_z\cdot\mathbf{e}_{b'})^2 - (\mathbf{e}_z\cdot\mathbf{e}_b)^2 - \mathbf{h}\cdot\mathbf{e}_b > 0. \qquad (30)$$

Here the linear term must vanish if the barrier direction is chosen properly: $A = 0$. This defines θ_b in $(\mathbf{e}_z\cdot\mathbf{e}_b) = \cos\theta_b$ and $(\mathbf{e}_z\cdot\mathbf{e}_{b'}) = \sin\theta_b$. For an arbitrarily directed $\mathbf{h}$, there is no analytical solution for θ_b, although it can be obtained numerically. Analytically solvable cases are

$$h_z = 0, \quad \theta_b = \pi/2, \quad B = 1 - h_x \qquad (31)$$

and

$$h_x = 0, \quad \cos\theta_b = -h_z, \quad B = 1 - h_z^2. \qquad (32)$$

One has to consider small nonuniform deviations from the barrier state, satisfying the boundary conditions $s'_\alpha = 0$ and orthogonal to a constant, and check whether they can reduce the energy. In fact, one can use the Fourier series for $\psi(z)$. The most dangerous perturbation is $\psi(z) = p\cos(\pi z/L_z)$. Substituting it into Eq. (29), one obtains

$$\delta E = \frac{1}{2}\mathcal{N}Dp^2\left(\frac{\pi^2\delta^2}{L_z^2} - B\right). \qquad (33)$$

This is positive and thus the SD state is stable for $L_z < \pi\delta/B$ which yields

$$L_z < \pi\delta\begin{cases}/\sqrt{1-h_x}, & h_z = 0,\\ /\sqrt{1-h_z^2}, & h_x = 0.\end{cases} \qquad (34)$$

For the periodic boundary conditions (e.g., for magnetic rings), the dangerous perturbation is $\psi = p\cos(2\pi z/L_z)$

which increases the exchange energy by a factor of four and makes the nonuniform solution more expensive. In this case the SD state is stable for $L_z < 2\pi\delta/B$.

For a particle of a cubic shape, there are similar instabilities with nonuniformities along the x, y, and z spatial axes. Nonuniformities along two or three axes at the same time cost too much exchange energy and are not viable. However, for larger particles, another mechanism, the nucleation near the surface, becomes important [19].

VII. VARIATIONAL SOLUTION IN THE TRANSITION REGION

To qualitatively study the transition between the uniform and nonuniform thermal activation, one can use the variational approach. In the simplest case of a zero field, the variational ansatz has the form

$$s_z = \tanh\left[p(z-z_0)\right], \quad s_x = 1/\cosh\left[p(z-z_0)\right], \tag{35}$$

where p is a variable parameter. These functions do not satisfy the boundary conditions. However, since the boundary conditions follow from the energy minimization, within the variational approach they can be discarded. The energy in our model, Eq. (20), for $\mathbf{h} = 0$ becomes

$$E = \mathcal{N}D\frac{1}{L_z}\int_0^{L_z} dz \frac{\delta^2 p^2 + 1}{\cosh^2\left[p(z-z_0)\right]}. \tag{36}$$

Integration yields

$$E = \mathcal{N}D\frac{1+\delta^2 p^2}{pL_z}\{\tanh[p(L_z - z_0)] + \tanh[pz_0]\}, \tag{37}$$

which has a flat maximum at $z_0 = L_z/2$, the DW in the center of the particle. This corresponds to the barrier height

$$U(p) = 2\mathcal{N}D\frac{1+\delta^2 p^2}{pL_z}\tanh\frac{pL_z}{2}. \tag{38}$$

This expression has to be minimized with respect to p. For $p \to 0$ this result recovers the barrier for the single-domain particle, $U_{SD} = \mathcal{N}D$. For $L_z \gg \delta$ the solution satisfies $pL_z \gg 1$, so that $\tanh(pL_z/2) \cong 1$. Then minimization yields $p = 1/\delta$ and U given by Eq. (7).

To study the transition between the two regimes, one can expand $U(p)$ as

$$\frac{U(q)}{\mathcal{N}D} \cong 1 + \left(1 - \frac{L_z^2}{12\delta^2}\right)(p\delta)^2 + \frac{L_z^2}{12\delta^2}\left(-1 + \frac{L_z^2}{10\delta^2}\right)(p\delta)^4. \tag{39}$$

Thus, the instability of the single-domain state within the variational approach sets in at $L_z = L_{z,c} = \sqrt{12}\delta \simeq 3.46\delta$ which differs from the exact criterion above by 10%. For $L_z > L_{z,c}$, the coefficient in front of the fourth-order term is positive; thus this is a second-order transition within the variational approach.

Using a similar method, one can study the transition from uniform to nonuniform barrier in the presence of transverse and longitudinal fields. Figure 10 shows the barrier vs L_z, relative to the domain-wall width δ. In the uniform region, the barrier grows linearly with the particle's volume, then it crosses over to a plateau. Transverse and longitudinal fields favor the uniform state; thus in the field, transition between the regimes happens at larger L_z.

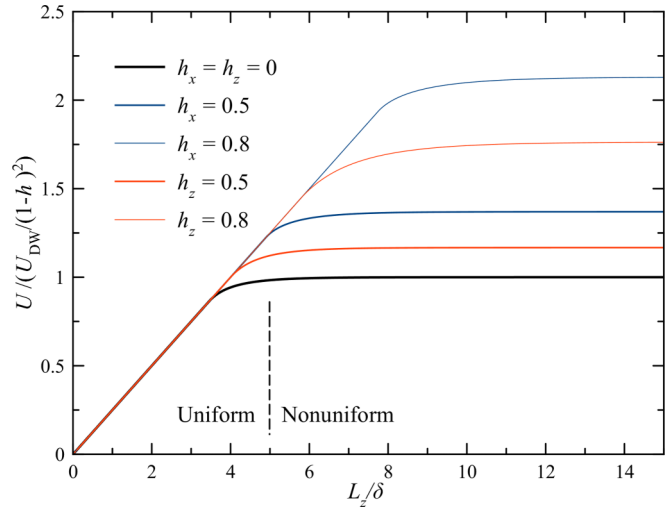

FIG. 10. Uniform-nonuniform crossover of the energy barrier on the magnetic particle's length L_z, relative to the domain-wall width δ.

VIII. DISCUSSION

It was shown that in the realistic case of weak damping, the pulse-noise approach to the solution of the Landau-Lifshitz-Langevin equation for spin systems coupled to a heat bath is efficient and can be used to compute thermally activated escape rates of magnetic nanoparticles in uniform and nonuniform switching regimes. It was found that single-domain magnetic particles show much higher switching rates than the equivalent single-spin models because of the internal thermal disordering manifesting itself in the temperature dependence of the effective anisotropy constant. The temperature dependence of the energy barrier was not a secret and it was understood that the apparent barriers extracted from the Arrhenius switching rates are the barriers at $T = 0$. The temperature corrections to the barriers strongly change the prefactors, so that a comparison with theoretical expressions is problematic.

Since thermal disordering of magnetic particles proves to be very important in their thermal switching, it is worth trying to take into account quantum-mechanical effects in the temperature dependence of the magnetization (e.g., the Bloch law). While obtaining a quantum-mechanical expression for the particle's magnetization from the quantum spin-wave theory seems to be possible, it is unclear how to make first-principle computations with quantum mechanics and Langevin fields.

It was demonstrated that for strong anisotropy at high temperature the magnetization switching is predominantly longitudinal with the magnetization reducing to zero at the barrier crossing. This is neither a uniform rotation nor a nonuniform rotation since at high temperatures the neighboring spins strongly deviate from collinearity in a random way.

At lower temperatures, the crossover from uniform (single-domain) rotation to nonuniform rotation by surmounting the barrier has been studied analytically, including the linear

instability boundary of the uniform barrier state. In the region of nonuniform rotation analytical expressions for the barriers in the presence of transverse and longitudinal field have been worked out. Computations using the pulse-noise method are in a good accordance with the values of the barriers, although in some cases the Arrhenius dependence with the given barrier sets in at pretty low temperatures (such as the curve $\lambda = 0.001$ in the lower panel of Fig. 9).

ACKNOWLEDGMENTS

This work has been supported by Grant No. DE-FG02-93ER45487 funded by the US Department of Energy, Office of Science.

APPENDIX: EXTRACTING ESCAPE RATES FROM ESCAPE DATA

The usual way to numerically compute escape rates is to run the numerical evolution routine until the particle crosses the barrier or using another stopping criterion like $m_z = 0$ and record the (first) passage time t_i for each ith run. The inverse of the mean first-passage time (MFPT), averaged over many runs, is identified with the escape rate, $\Gamma = 1/\langle t_i \rangle$.

The mathematics behind this relies on the assumption that the probability for a particle to stay in the initial state decreases exponentially with time: $P(t) = e^{-\Gamma t}$. This is the unnormalized distribution of passage times, so that the mean passage time is given by $\mathrm{MFPT} = \Gamma \int_0^\infty dt\, t P(t) = 1/\Gamma$, where Γ in front of the integral normalizes the distribution. This confirms the validity of the standard method of extracting Γ.

A drawback of this method to extract Γ is that absolutely all particles must escape. If the preset computation time was too short and not all particles escaped, the efforts have been wasted and the computation has to be repeated. Increasing the preset computation time leads to very long computations at the lowest temperatures as the distribution of passage times becomes broad and there are extremely long-lived particles.

A more advanced method is to consider the sorted list of passage times t_i and identify i with the number of particles already escaped by the time t_i. Then the probability to escape by the time t_i becomes i/N, where N is the total number of runs used in the computation, i.e., the total number of particles. Thus the staying probability at t_i can be expressed as

$$P(t_i) = 1 - \frac{i}{N}. \tag{A1}$$

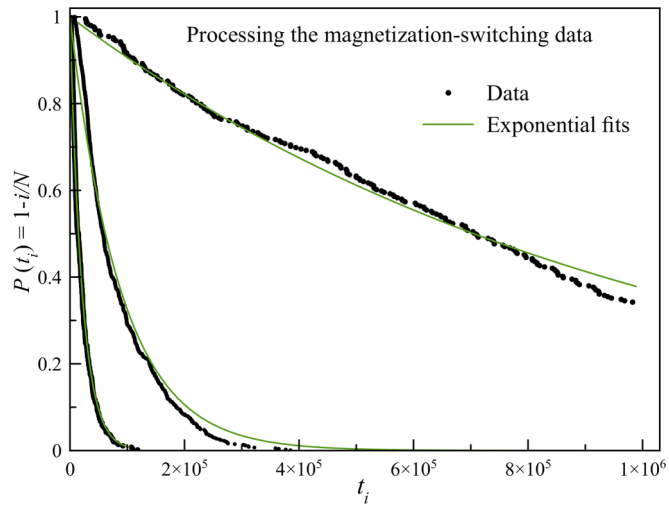

FIG. 11. Extracting escape rates from escape data. This method does not require all particles to escape.

Assuming that $P(t)$ is exponential, one can fit the list $\{t_i, P(t_i)\}$ with the exponential function to extract Γ. Since fitting is a nonlinear procedure, it can fail; thus it is better to be avoided. Instead of the fitting, one can extract Γ by resolving the exponential as $\Gamma = -\ln P(t)/t$. This results in the formula used in this work, as well as in Ref. [24]:

$$\Gamma = -\left\langle \frac{1}{t_i} \ln\left(1 - \frac{i}{N}\right)\right\rangle. \tag{A2}$$

This formula gives practically the same values of Γ as the exponential fits shown in Fig. 11. Here the averaging includes only those particles that escaped, whereas N is the total number of particles. This formula is robust and does not require all particles to escape. To the contrary, limiting the preset computation time allows one to speed up the computations at the lowest temperatures extracting the information from the subset of the shortest-lived particles. The latter amounts to determining the exponential by its initial part, as can be seen in Fig. 11.

In these computations, the preset computation time was $t_{\max} = 10^6$. With the standard method of data processing, this would allow one to compute escape rates significantly higher than $1/t_{\max}$, say, down to $\Gamma = 10^{-5}$. With the current method, escape rates down to $\Gamma = 10^{-7}$ have been computed.

Another advantage of this method is the possibility of plotting the staying probability, as is done in Fig. 11 to check whether it is exponential. In particular, at high temperatures this curve is more resembling a Gaussian; thus the extracted Γ are only approximate.

[1] W. F. Brown, Jr., *Micromagnetics* (Interscience, New York, 1963).

[2] H. Kronmüller and S. Parkin, editors, *Handbook of Magnetism and Advanced Magnetic Materials*, Vol. 2 (Wiley, New York, 2007).

[3] R. Dittrich, T. Schrefl, D. Suess, W. Scholz, H. Forster, and J. Fidler, J. Magn. Magn. Mater. **250**, 12 (2002).

[4] Weinan E, W. Ren, and E. Vanden-Eijnden, Phys. Rev. B **66**, 052301 (2002).

[5] J. Xue and R. H. Victora, J. Appl. Phys. **89**, 6985 (2001).

[6] G. Ziemys, S. Breitkreutz-v. Gamm, G. Csaba, D. Schmitt-Landsiedel, and M. Becherer, AIP Adv. **7**, 056625 (2017).

[7] E. Martinez, L. Lopez-Diaz, L. Torres, and C. Garcia-Cervera, J. Magn. Magn. Mater. **316**, 269 (2007).

[8] L. D. Landau and E. M. Lifshitz, Phys. Z. Sowjetunion **8**, 153 (1935).
[9] D. A. Garanin, Phys. Rev. B **55**, 3050 (1997).
[10] O. Chubykalo-Fesenko, U. Nowak, R. W. Chantrell, and D. A. Garanin, Phys. Rev. B **74**, 094436 (2006).
[11] W. F. Brown, Jr., Phys. Rev. **130**, 1677 (1963).
[12] W. T. Coffey, D. S. F. Crothers, J. L. Dormann, Y. P. Kalmykov, E. C. Kennedy, and W. Wernsdorfer, Phys. Rev. Lett. **80**, 5655 (1998).
[13] Y. P. Kalmykov and W. T. Coffey, J. Appl. Phys. **112**, 121301 (2012).
[14] A. Lyberatos and R. W. Chantrell, J. Appl. Phys. **73**, 6501 (1993).
[15] J. L. García-Palacios and F. J. Lázaro, Phys. Rev. B **58**, 14937 (1998).
[16] D. A. Garanin and H. Kachkachi, Phys. Rev. Lett. **90**, 065504 (2003).
[17] R. Yanes, O. Chubykalo-Fesenko, H. Kachkachi, D. A. Garanin, R. Evans, and R. W. Chantrell, Phys. Rev. B **76**, 064416 (2007).
[18] H. Kachkachi and D. A. Garanin, in *Surface Effects in Magnetic Nanoparticles*, edited by D. Fiorani (Springer, Boston, MA, 2004).
[19] D. Hinzke and U. Nowak, Phys. Rev. B **58**, 265 (1998).
[20] O. Chubykalo, J. D. Hannay, M. Wongsam, R. W. Chantrell, and J. M. Gonzalez, Phys. Rev. B **65**, 184428 (2002).
[21] H.-J. Suh, C. Heo, C.-Y. You, W. Kim, T.-D. Lee, and K.-J. Lee, Phys. Rev. B **78**, 064430 (2008).
[22] R. Bastardis, U. Atxitia, O. Chubykalo-Fesenko, and H. Kachkachi, Phys. Rev. B **86**, 094415 (2012).
[23] R. F. L. Evans, W. J. Fan, P. Chureemart, T. A. Ostler, M. O. A. Ellis, and R. W. Chantrell, J. Phys.: Condens. Matter **26**, 103202 (2014).
[24] D. A. Garanin, Phys. Rev. E **95**, 013306 (2017).
[25] D. Hinzke and U. Nowak, Phys. Rev. B **61**, 6734 (2000).
[26] G. Bertotti, I. Mayergoyz, and C. Serpico, *Nonlinear Magnetization Dynamics in Nanosystems* (Elsevier, Amsterdam, 2009).
[27] I. Mayergoyz, G. Bertotti, and C. Serpico, Phys. Rev. B **83**, 020402 (2011).
[28] D. A. Garanin, V. V. Ishchenko, and L. V. Panina, Teor. Mat. Fiz. **82**, 169 (1990).
[29] W. T. Coffey and Y. P. Kalmykiv, *The Langevin Equation* (World Scientific, Singapore, 2004).
[30] E. C. Stoner and E. P. Wohlfarth, Philos. Trans. R. Soc. London, Ser. A **240**, 599 (1948).
[31] E. C. Stoner and E. P. Wohlfarth, IEEE Trans. Magn. **MAG-27**, 3475 (1991).
[32] L. Néel, Ann. Geophys. (C.N.R.S.) **5**, 99 (1949).
[33] D. A. Garanin, E. C. Kennedy, D. S. F. Crothers, and W. T. Coffey, Phys. Rev. E **60**, 6499 (1999).
[34] J. S. Broz, H. B. Braun, O. Brodbeck, W. Baltensperger, and J. S. Helman, Phys. Rev. Lett. **65**, 787 (1990).
[35] H. B. Braun and H. N. Bertram, J. Appl. Phys. **75**, 4609 (1994).
[36] H.-B. Braun, Phys. Rev. B **50**, 16501 (1994).
[37] Y. P. Kalmykov, Phys. Rev. E **62**, 227 (2000).
[38] U. Nowak, R. W. Chantrell, and E. C. Kennedy, Phys. Rev. Lett. **84**, 163 (2000).
[39] O. Chubykalo, U. Nowak, R. Smirnov-Rueda, M. A. Wongsam, R. W. Chantrell, and J. M. Gonzalez, Phys. Rev. B **67**, 064422 (2003).
[40] H. Kachkachi and D. A. Garanin, Physica A **300**, 487 (2001).
[41] N. Akulov, Z. Phys. **100**, 197 (1936).
[42] D. A. Garanin and O. Chubykalo-Fesenko, Phys. Rev. B **70**, 212409 (2004).
[43] R. F. L. Evans, D. Hinzke, U. Atxitia, U. Nowak, R. W. Chantrell, and O. Chubykalo-Fesenko, Phys. Rev. B **85**, 014433 (2012).
[44] H. Kachkachi and D. A. Garanin, Physica A **291**, 485 (2001).
[45] N. Kazantseva, D. Hinzke, R. W. Chantrell, and U. Nowak, Europhys. Lett. **86**, 27006 (2009).
[46] L. N. Bulaevskii and V. L. Ginzburg, Zh. Eksp. Teor. Fiz. **45**, 772 (1963) [Sov. Phys. JETP **18**, 530 (1964)].
[47] J. Kötzler, D. A. Garanin, M. Hartl, and L. Jahn, Phys. Rev. Lett. **71**, 177 (1993).
[48] M. Hartl-Malang, J. Kötzler, and D. A. Garanin, Phys. Rev. B **51**, 8974 (1995).
[49] D. A. Garanin and H. Kachkachi, Phys. Rev. B **80**, 014420 (2009).
[50] D. A. Garanin, Physica A **178**, 467 (1991).
[51] See Supplemental Material at http://link.aps.org/supplemental/10.1103/PhysRevB.98.144425 for videos of thermal switching of spin chains in the various regimes considered.